Three Dimensional and Two Phase Modeling of a Flowing Electrolyte – Direct Methanol Fuel Cell

*O. Faruk Atacan, D. Ouellette, C.O. Colpan

[1]*Dokuz Eylül University, Faculty of Engineering, Mechanical Engineering Department, İzmir, 35397, Turkey

* E-mail: farukatacann@hotmail.com

Abstract

Direct methanol fuel cell is a promising candidate for portable applications since its fuel is in the liquid state at low temperatures, allowing for an energy dense and inexpensive fuel that can easily be stored. Nonetheless, the problem of methanol crossover, which is from anode to cathode is one of the main problem for commercialization of this fuel cell. In order to prevent this methanol crossover, Kordesch proposed the flowing electrolyte concept, whereby the anode and cathode are separated by a flowing liquid electrolyte, such as diluted sulfuric acid. This concept is known as the flowing electrolyte – direct methanol fuel cell or FE-DMFC. By means of this concept, the methanol, which tries to reach to the cathode side can be blocked by the flowing electrolyte channel, which nearly prevents this electrochemical short circuit. Many researchers have modelled this type of fuel cell; however the majority of studies included a single phase model and examined the performance of the FE-DMFC under different operating conditions. Recently a two-phase model of the FE-DMFC has been developed using a single-domain formulation of the multiphase mixture model (MMM) and two phase non-isothermal model which was extended the single domain as two-dimensional. Owing to the more realistic modeling predictions of the multiphase model, the single domain formulation is extended to account for 3D within the FE-DMFC. This three-dimensional and two phase model is first used to investigate the concentration distribution of methanol and saturation at the baseline condition. Then, the effect of FEC thickness is investigated for four different values of FEC thicknesses at 0.5 V cell voltage. The results show that FEC thickness should be 0.4 mm for the given set of data. At this thickness, the negative effects of methanol crossover are minimized and the power density is maximized.

Keywords: DMFC, Comsol Multiphysics, FE-DMFC, simulation, two phase

I. Introduction

Fuel cells are electrochemical devices that convert chemical energy directly into electrical energy. They can be used in power generation, as well as in a portable application. For portable application, direct methanol fuel cell (DMFC) is a promising candidate which uses liquid methanol as fuel because of its easy storage, low price, and high power density ((C.O. Colpan, I. Dincer, 2008)). This type of fuel cell is composed of several layers (shown in Fig.1). The operating principle of the DMFC is as follows: Diluted methanol solution is supplied at the anode fuel channel (AFC) inlet and diffused through the ABL (e.g. carbon cloth or carbon paper) to the ACL (e.g. Pt-Ru/C). At this layer, the electrochemical reaction, shown in Eq. (1) occurs. The electrons and protons generated move in opposite directions. The protons are conducted through the membrane (e.g. Nafion®) to the CCL; whereas the electrons pass through the ABL, external load, CBL and reach the CCL (e.g. Pt/C). In this layer, they react with the oxygen diffused through the air channel and CBL (e.g. carbon cloth or carbon paper) as can be seen in Eq. (2). In addition to this reaction, methanol crossing over through the membrane also react with oxygen, Eq. (3), which reduces the active area for the reaction shown in Eq. (2); and this undesired crossover causes an additional voltage loss.

$$CH_3OH + H_2O \rightarrow CO_2 + 6H^+ + 6e^- \quad (1)$$

$$1.5O_2 + 6H^+ + 6e^- \rightarrow 3H_2O \quad (2)$$

$$CH_3OH + 1.5O_2 \rightarrow CO_2 + 2\,H_2O \quad (3)$$

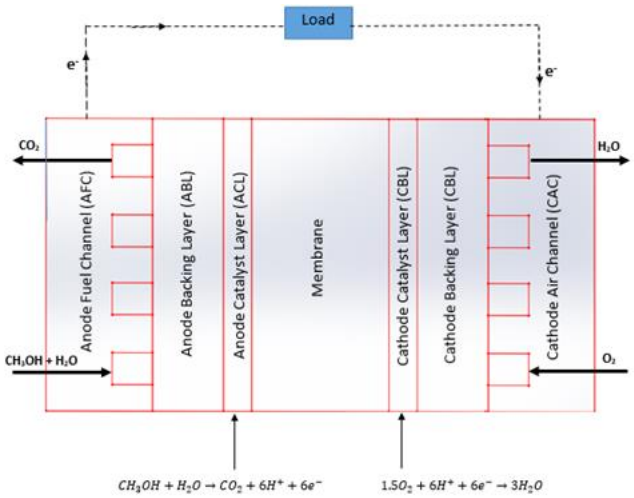

Fig. 1. Schematic representation of the DMFC

DMFC has some shortcomings such as low electrochemical reaction rate on the anode side, water management problem and high cost of catalysts (e.g. Pt). However, the methanol crossover problem is one of the biggest obstacle towards the commercialization

of this type of fuel cell. Methanol crossover is the undesired methanol transition from anode to the cathode which causes a reduction in fuel cell's power density, electrical efficiency and voltage drop. In order to prevent these negative effects, the flowig electrolyte concept was proposed by Kordesch et al. (2001). By this concept, anode and cathode are separated with flowing liquid electrolyte (e.g. sulfuric acid). Any methanol that attempts to crossover is removed from the system, hence protecting the CCL. The schematic of this new flowing electrolytic concept with direct methanol fuel cell is shown in Fig. 2. This system is also known as flowing electrolye direct methanol fuel cell (FE-DMFC).

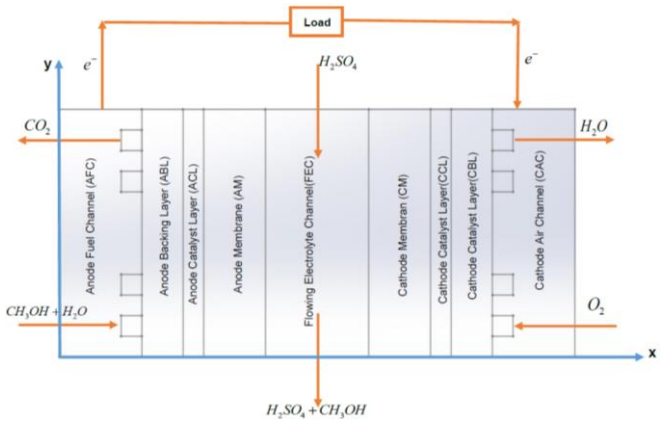

Fig. 2. Schematic of the FE-DMFC

Numerous single phase studies and models on the FE-DMFC are found in the literature. Methanol crossover reduction in the flowing electrolyte channel with different operating parameters, through three dimensional (3D) modeling was studied by Kjeang et al. (Kjeang et al., 2005, 2006). 1D and 2D models of the FE-DMFC were devolep to predict the performance of the fuel cell under different operating conditions and fuel, air, and FEC inlet velocities by Colpan et al. (2011, 2012). Colpan's one-dimensional FE-DMFC model was extended to predict how the performance changes with the inlet concentration of the FE, as well as the flow rate and thickness of the flowing electrolyte channel (FEC) by Ouellette et al. (2015). Sabet-Sharghi et al. (2013) studied the performance of a single cell FE-DMFC and compared it to regular DMFC. Duivesteyn et al. (2013, 2013) modelled the flowing electrolyte layer, by as a porous domain in ANSYS CFX. General flow behaviour and the effects of volume flux, temperature, channel thickness, and porous material properties were investigated. Kablou et al. (2015) experimentally and numerically studied the FE-DMFC stack . Colpan et al. (2017) experimentally studied the methanol crossover reduction in FE-DMFC and the performances of the FE-DMFCs were compared with those of the DMFCs having a single or double membrane.

Although, there are several single phase studies on the FE-DMFC, there are limited studies on the multiphase modelling of the FE-DMFC. Ouellette et al. (2015a, 2015b) improved the multi mixture model (Jung (2013); Liu & Wang (2007); Wang and Wang, (2003)) approach by developing a new single domain FE-DMFC model. To find the maximum power density and minimal methanol and water crossover, a parametric study was conducted. Atacan et al. (2016) developed a 2D multiphase non-isothermal model of a FE-DMFC and found that if the inlet temperatures of the anode or cathode are too low, possible flooding could occur within the air channel.

Literature survey conducted shows that there are no studies on the 3D multiphase modelling of FE-DMFC. Hence, to understand the FE-DMFC further, Ouellette et al.'s (2015) MMM model is extended to account for the multidimensional effects. Developed model shows us how the species concentration (methanol and saturation) changes within the complete cell geometry. The effect of FEC thickness on the fuel cell performance is also investigated as a parametric study.

II. Modeling

A three dimensional two phase model of a FE-DMFC has been developed. In this model, Ouellette et al.'s (2015) single domain MMM model has been extended. To develop the model, the conservation equations (mass, momentum, chemical species and charge) and other auxiliary equations (e.g. Butler-Volmer equation) are coupled together and solved using COMSOL Multiphysics, which is a commercial software package based on finite element analysis. The main assumptions used in the modeling are as follows.

- The fuel cell operates under steady state conditions.
- Methanol is fully consumed at the CCL-CBL interface.
- The inlet FEC velocity profile is uniform
- The BLs and CLs have the same porous properties.
- All fluids are ideal and exist in equilibrium.

The governing equations used in model, mass (Eq. (4)), momentum (Eq. (5)), species (Eq. (6)), and charge (Eqs. (7) and (8)) are presented in succinct form as follows:

$$\nabla \cdot (\rho \mathbf{u}) = S_{gen} + S_{trans} \tag{4}$$

$$\frac{\rho}{\varepsilon_p}\left[(\nabla \cdot \mathrm{u})\frac{\mathrm{u}}{\varepsilon_p}\right] = \nabla \cdot \left[-P\mathrm{I} + \frac{\mu}{\varepsilon_p}\left\langle(\nabla \mathrm{u}) + (\nabla \mathrm{u})^T\right\rangle - \frac{2\mu}{3\varepsilon_p}(\nabla \cdot \mathrm{u})\mathrm{I}\right] - \left(\frac{\mu}{K} + \beta|\mathrm{u}| + \frac{S_{gen}}{\varepsilon_p^2}\right)\mathrm{u} + \mathrm{f} \tag{5}$$

$$\nabla \cdot \left[-D_{\mathrm{lg}}^k(\nabla C_i^k) + \mathbf{u}_{\mathbf{lg}}^{\mathbf{k}} C_i^k\right] = S_{gen}^k + S_{trans}^k \tag{6}$$

$$\nabla \cdot \left[-\sigma_l \left(\nabla \phi_l \right) \right] = S_{c,l} \quad (7)$$

$$\nabla \cdot \left[-\sigma_s \left(\nabla \phi_s \right) \right] = S_{c,s} \quad (8)$$

To account for the mixture velocity (u) and pressure distribution, Eqs. (4) and (5) are directly coupled together. This mixture velocity is then used to calculate the convective mode of transport within Eqs. (6) and (7). The concentration profile of each species (methanol, water, oxygen) is obtained from Eq. (6) and the current distributions are obtained from Eqs. (7) and (8).

A summary of the fuel cell geometry parameters, two-phase diffusion coefficients, D_{lg}^{k}, and velocities, $\mathbf{u}_{\mathrm{lg}}^{k}$, boundary conditions, source terms (S_{gen}^{k} , $S_{c,l}$, $S_{c,s}S_{trans}$), constitutive electrochemical and mixture equations, material properties and electrochemical transport properties used in modeling study are respectively shown in Tab. 1-8.

II.I Numerical procedure

COMSOL Multiphysics 5, which is based on finite element methods is used to solve the governing equations (Eqs. 4-9). The following built-in modules have been used.

- The Transport of Diluted Species in Porous Media interface to solve the oxygen, water and methanol concentration fields.
- The Secondary Current Distribution interface to solve the charge transport equations.
- The Free and Porous Media Flow interface to solve the Navier-Stokes and continuity equations.

To obtain a mesh-independent model, the change in the value of the current density is determined by increasing the mesh at certain intervals for each layer. The mesh number is increased regularly until the error margin between the two values is less than 0.1%. If the error margin falls below this value, the number of meshes is determined as the number of meshes of that layer. This process is applied step by step for all layers and the independence of the mesh is ensured. As a result of this process, the total number of mesh is found as 1200000. In order to save time in calculations, symmetry condition is given at the center of the fuel cell to reduce the number of meshes (as shown in Fig.3). In addition, the maximum element size is set to 0.0042 m and the maximum element grow rate is set to 1.5. The stationary nonlinear setting is used and each governing equation is solved sequentially using a direct solver, specifically MUMPS (multifrontal massively parallel sparse direct solver) due to the nonlinearity of the equations.

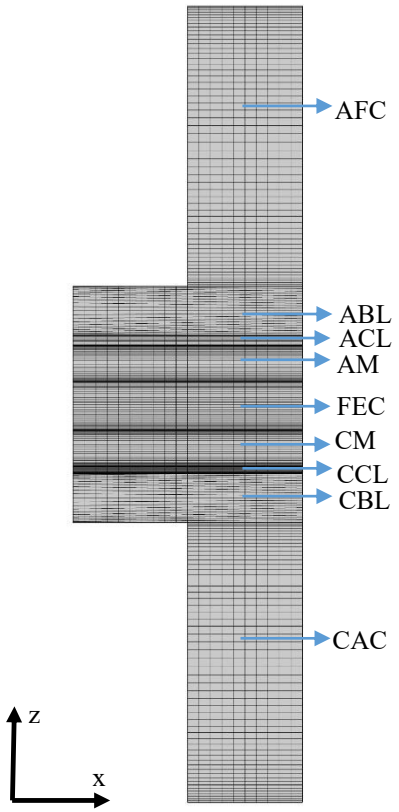

Fig. 3 – Meshing in Comsol

Tab.1. Fuel cell geometry.

Parameter	Value	Units
Cell Length	42×10^{-3}	m
Active Area	$1.764\text{x}10^{-3}$	m^2
Thickness		
ABL and CBL	0.175×10^{-3}	m
AFC and CAC	$1\text{x}10^{-3}$	m
AM and CM	0.127×10^{-3}	m
FEC	0.175×10^{-3}	m
ACL and CCL	$38\text{x}10^{-6}$	m
Channel Dimensions		
Width	$1.5\text{x}10^{-3}$	m
Depth	$1\text{x}10^{-3}$	m

Tab. 2. Two phase diffusion coefficient and velocity

Species	D_{lg}^{k}	$\mathbf{u}_{\mathrm{lg}}^{k}$
Methanol	$D_l^{MeOH}+\frac{D_g^{MeOH}}{k_H^{MeOH}}+D_e^{MeOH}$	$\gamma^{MeOH}\mathbf{u}\left(s+\frac{1-s}{k_H^{MeOH}}\right)+\mathbf{j_l}\left(\frac{1}{\rho_l}-\frac{1}{k_H^{MeOH}\rho_g}\right)+\left(\varepsilon_e\frac{n_d^{H_2O}}{C_l^{H_2O}}\frac{\mathbf{i_e}}{F}\right)$
Oxygen	$D_g^{O_2}$	$\gamma^{O_2}\mathbf{u}(1-s)-\frac{\mathbf{j_l}}{\rho_g}$
Water	$\begin{cases} D_g^{H_2O}+D_{\lambda,eff}^{H_2O}\ldots\ldots C^{H_2O}\le C_{g,sat}^{H_2O} \\ D_{cap}^{H_2O}+D_{\lambda,eff}^{H_2O}\ldots\ldots C_{g,sat}^{H_2O}\le C^{H_2O}\le C_l^{H_2O} \\ D_l^{H_2O}+D_{\lambda,eff}^{H_2O}\ldots\ldots C^{H_2O}=C_l^{H_2O} \end{cases}$	$\gamma^{H_2O}\mathbf{u}$

Tab. 3. Boundary conditions used within the model.

Boundary condition	Location	Symbol	Value	Units
Molar concentration				
MeoH	AFC-ABL	$C_{FC,in}^{MeoH}$	1000	mol m^{-3}
	CCL-CBL	$C_{CCL\|CBL}^{MeoH}$	0	mol m^{-3}
O_2	CBL-AC	$C_{FC,in}^{O_2}$	$x_{O_2}\frac{P_{ac,in}}{RT}$	mol m^{-3}
H_2O	AFC-ABL	$C_{AFC\|ABL}^{H_2O}$	$s_aC_l^{H_2O}+(1-s_a)C_g^{H_2O}$	mol m^{-3}
	CAC-CBL	$C_{CAC\|CBL}^{H_2O}$	$s_cC_l^{H_2O}+(1-s_c)C_g^{H_2O}$	mol m^{-3}
Electrode phase potential				
	FC-ABL	$\phi_{s,FC\|ABL}$	0	V
	ABL-AC	$\phi_{s,CBL\|AC}$	V_{cell}	V
Inlet velocities				
	AFC Inlet	$\mathbf{u}_{\mathbf{FC,in}}$	$\frac{\xi_a i_{ref}A}{6FC_{FC,in}^{MeOH}A_{channel}}$	m s^{-1}
	CAC Inlet	$\mathbf{u}_{\mathbf{AC,in}}$	$\frac{\xi_c i_{ref}A}{4FC_{FC,in}^{O_2}A_{channel}}$	m s^{-1}
	FEC Inlet	$\mathbf{u}_{\mathbf{FEC,in}}$	$\frac{Q_{FEC}}{w_{cell}t_{FEC}}$	m s^{-1}
Outlet pressures				
Anode	Anode outlet	$P_{a,out}$	1	atm
Cathode	Cathode outlet	$P_{c,out}$	1	atm
FEC	FEC outlet	$P_{FEC,out}$	1	atm

Tab.4. Summary of source terms.

Source/ Sink Terms	Expression						
	ABL	ACL	AM	FEC	CM	CCL	CBL
S_{gen}^{MEOH}	0	$-\frac{j}{6F}$	0	0	0	0	0
$S_{gen}^{O_2}$	0	0	0	0	0	$-\frac{j}{4F}-2\frac{j_{xover}}{6F}$	0
$S_{gen}^{H_2O}$	0	$-\frac{j}{6F}-\nabla\left(\varepsilon_e n_d^{H_2O}\frac{\mathbf{i_e}}{F}\right)$	$-\nabla\left(\varepsilon_e n_d^{H_2O}\frac{\mathbf{i_e}}{F}\right)$	$-\nabla\left(\varepsilon_e n_d^{H_2O}\frac{\mathbf{i_e}}{F}\right)$	$-\nabla\left(\varepsilon_e n_d^{H_2O}\frac{\mathbf{i_e}}{F}\right)$	$\frac{j}{2F}+2\frac{j_{xover}}{6F}-\nabla\left(\varepsilon_e n_d^{H_2O}\frac{\mathbf{i_e}}{F}\right)$	0
$S_{gen}^{CO_2}$	0	$\frac{j}{6F}$	0	0	0	$\frac{j_{xover}}{6F}$	0
S_{trans}	CLs						
	$\nabla.\left[D_{\lambda,eff}^{H_2O}M^{H_2O}(\nabla C^{H_2O})+D_e^{MeOH}M^{MeOH}(\nabla C_l^{MeOH})-M^{MeOH}\nabla.\left(\varepsilon_e\frac{n_d^{MeOH}}{C_l^{MeOH}}\frac{i}{F}\right)C_l^{MeOH}-M^{H_2O}\nabla.\left(\varepsilon_e\frac{n_d^{H_2O}}{C_l^{H_2O}}\frac{i}{F}\right)C_l^{H_2O}\right]$						

Tab.5. Constitutive electrochemical equations.

Constitutive equations	Expression
Anodic Non-Tafel expression	$j_a=\frac{i_{oa,ref}C^{MeOH}\exp\left(\frac{\alpha_a F}{RT}\eta_a\right)}{\left(\left(C^{MeOH}+K_a\exp\left(\frac{\alpha_a F}{RT}\eta_a\right)\right)*t_{ACL}\right)}$
Cathodic Tafel expression	$j_c+j_{xover}=\frac{i_{oc,ref}(1-s)\frac{C^{O_2}}{C_{ref}^{O_2}}\exp\left(\frac{\alpha_c F}{RT}\eta_c\right)}{t_{CCL}}$
Anodic overpotential	$\eta_a=\phi_s-\phi_l-E_a^{Eq}$
Cathodic overpotential	$\eta_c=-(\varphi_s-\varphi_l-E_c^{Eq})$
Crossover current density	$j_{xover}=\frac{i_{oa,ref}C^{MeOH}\exp\left(\frac{\alpha_a F}{RT}\eta_c\right)}{\left(\left(C^{MeOH}+K_a\exp\left(\frac{\alpha_a F}{RT}\eta_c\right)\right)*t_{ACL}\right)}$

Tab.6. Constitutive mixture equations.

Variable	Expression
Mixture density	$\rho = s\rho_l + (1-s)\rho_g$
Molar mixture concentration	$C^k = sC_l^k + (1-s)C_l^k$
Kinematic mixture viscosity	$\nu = \left[\frac{k_{rl}}{\nu_l} + \frac{k_{rg}}{\nu_g}\right]^{-1}$
Relative permeability	$k_{rl} = s^3$ $k_{rg} = (1-s)^3$
Relative mobility	$\lambda = k_{rl}\frac{\nu}{\nu_l}$ $\sum_i \lambda_i = 1$
Advection correction factor	$\gamma^k = \frac{\rho}{C^k}\left[\lambda\frac{C_l^k}{\rho_l} + (1-\lambda)\frac{C_g^k}{\rho_g}\right]$
Capillary diffusion flux	$\mathbf{j_l} = \frac{\lambda(1-\lambda)K}{\nu}\left(\nabla P_{cap}\right)$
Mixture mass flux	$(\rho\mathbf{u}) = (\rho\mathbf{u})_\mathbf{l} + (\rho\mathbf{u})_\mathbf{g}$
Individual phase mass flux	$(\rho\mathbf{u})_\mathbf{i} = \mathbf{j_i} + \lambda_i(\rho\mathbf{u})$
Capillary pressure	$P_{cap} = \sigma(\cos\theta_c)\left(\frac{\varepsilon}{K}\right)^{\frac{1}{2}} J$
Leverett J-function	$J = 1.417s - 2.120s^2 + 1.263s^3$

Tab. 7. Fuel cell dimensions and material properties used in modeling study (Atacan et al. 2016)

Parameter	Symbol	Value	Units
Porosity			
AFC and CAC	ε_{AFC} and ε_{CAC}	1	-
ABL and CBL	ε_{ABL} and ε_{CBL}	0.78	-
ACL and CCL	ε_{ACL} and ε_{CCL}	0.78	-
AM and CM	ε_{AM} and ε_{CM}	0.28	-
FEC	ε_{FEC}	0.78	-
Electrolyte volume fraction			
ACL and CCL	$\varepsilon_{e,ACL}$ and $\varepsilon_{e,CCL}$	0.2	-
AM, CM and FEC	$\varepsilon_{e,AM}$ and $\varepsilon_{e,CM}$ and $\varepsilon_{e,FEC}$	1.0	-
Permeability			
ABL and CBL	K_{ABL} and K_{CBL}	$1.0\text{x}10^{-12}$	m^2
ACL and CCL	K_{ACL} and K_{CCL}	$1.0\text{x}10^{-12}$	m^2
AM and CM	K_{AM} and K_{CM}	$1.0\text{x}10^{-18}$	m^2
FEC	K_{FEC}	$1.0\text{x}10^{-11}$	m^2
Contact angle			
ABL and CBL	$\theta_{c,ABL}$ and $\theta_{c,CBL}$	110	degrees
ACL and CCL	$\theta_{c,ACL}$ and $\theta_{c,CCL}$	110	degrees
AM and CM	$\theta_{c,AM}$ and $\theta_{c,CM}$	90.01	degrees
FEC	$\theta_{c,FEC}$	110	degrees
Electrolyte density			
ABL and CBL	$\rho_{e,ACL}$ and $\rho_{e,CCL}$	1980	kg m^{-3}
ACL and CCL	$\rho_{e,AM}$ and $\rho_{e,CM}$	1980	kg m^{-3}
Electrolyte equivalent weight			
ABL and CBL	$M_{e,ACL}$ and $M_{e,CCL}$	1.1	kg mol^{-1}
ACL and CCL	$M_{e,AM}$ and $M_{e,CM}$	1.1	kg mol^{-1}

Tab. 8. Electrochemical and transport properties used in modeling study (Atacan et al., 2016)

Parameter	Symbol	Expression	Units
Diffusion coefficients			
MeOH in water	$D_{o,l}^{MeOH}$	$1.58x10^{-9}\exp\left[0.02623\left(T-298.15\right)\right]$	$m^2\ s^{-1}$
MeOH in gas	$D_{o,g}^{MeOH}$	$1.96x10^{-5}\left(\frac{T}{328.15}\right)^{1.823}$	$m^2\ s^{-1}$
MeOH in Nafion	D_e^{MeO}	$10^{-10}\left(0.12\lambda_{wc}+2.58\right)\exp\left[\left(-2882+14.126\lambda_{wc}\right)\left(\frac{1}{T}-\frac{1}{298.15}\right)\right]$	$m^2\ s^{-1}$
Water in gas	$D_{o,g}^{H_2O}$	$2.56x10^{-5}\left(\frac{T}{307.15}\right)^{2.334}$	$m^2\ s^{-1}$
Water in Nafion	$D_e^{H_2O}$	$4.17x10^{-8}\lambda_{wc}\left[1+161\exp\left(-\lambda_{wc}\right)\right]\exp\left(\frac{-2436}{T}\right)$	$m^2\ s^{-1}$
Oxygen in gas	$D_{o,g}^{O_2}$	$1.775x10^{-5}\left(\frac{T}{328.15}\right)^{1.823}$	$m^2\ s^{-1}$
Henry's Law coefficients for methanol	k_H^{MeOH}	$2.2\bar{R}T\exp\left[5200\left(\frac{1}{T}-\frac{1}{298.15}\right)\right]$	-
Reversible cell voltage	V_{rev}	$1.213-(1.4x10^{-4})(T-298.15)$	V
Coefficient of electro-osmatic drag (EOD)			
Coefficient of (EOD) of water	$n_d^{H_2O}$	$\begin{cases}\left(\frac{\lambda_{wc}-14}{18}\right)\left(n_{d,ref}^{H_2O}-1\right)+1 \ldots\ldots \lambda_{wc}\geq 14\\ 1\ldots\ldots \lambda_{wc}\leq 14\end{cases}$	-
Reference coefficient of EOD	$n_{d,ref}^{H_2O}$	$1.6767+0.0155(\mathrm{T}\text{-}273.15)+(8.9074\mathrm{x}10^{-5})(\mathrm{T}\text{-}273.15)^2$	-
Proton conductivity			
AM and CM	κ_{AM} and κ_{CM}	$\left(0.5139\lambda_{wc}+0.326\right)\exp\left[-1268\left(\frac{1}{T}-\frac{1}{303.15}\right)\right]$	$S\ m^{-1}$
FEC	κ_{FEC}	$(\mathrm{-1.26x10^{-3}})\mathrm{T}^2+(1.05032)\mathrm{T}-173.164$	$S\ m^{-1}$
Methanol oxidation reaction consatant	K_a	$2.265x10^{-3}$	$mol\ m^{-3}$
Reference oxygen concentration	$C_{ref}^{O_2}$	$0.21\frac{P}{RT}$	$mol\ m^{-3}$
Contact resistance	$R_{contact}$	$8x10^{-5}$	$ohm\ m^2$
Transfer coefficient			
Anode	α_a	0.5000	-
Cathode	α_c	0.9052	-
Reference exchange current density			
Anode	$i_{oa,\ ref}$	$0.9570\exp\left[-\frac{35570}{R}\left(\frac{1}{T}-\frac{1}{353.15}\right)\right]$	$A\ m^{-2}$
Cathode	$i_{oc,\ ref}$	$0.0204\exp\left[-\frac{73200}{R}\left(\frac{1}{T}-\frac{1}{353.15}\right)\right]$	$A\ m^{-2}$

III. Results and discussions

A 3D and two-phase model has been developed to investigate the methanol concentration and saturation distrubition in a FE-DMFC. In the baseline conditions, the fuel cell operates at 80°C, with 1 M methanol solution at the anode inlet and 101325 Pa air at the cathode inlet. The stoichiometric flow ratios at the anode and cathode flow channels are set to 2 and 3, respectively. In order to understand the numerical

results shown in this section distinctly, two 3D (shown in Figs. 4,6.) and three 1D plots(shown in Figs. 5, 7 ,8) are presented.

III. I. Baseline condition

The methanol concentration distributions are shown in Fig. 4, for a cell voltage of 0.2 V (i =1926.4 A m^{-2}). The methanol concentration decreases along the length-wise (y-direction) and thickness-wise (z-direction) directions owing to the increased consumption of methanol within ACL. The production of protons in the ACL (shown in Eq.1) causes the electro-osmotic drag of methanol through the membrane. In the FEC, the methanol concentration considerably decreases due to the convective crossflow as shown in Fig. 5., reducing the crossover current density, with a maximum of ~30 A m^{-2} at 0.5 V.

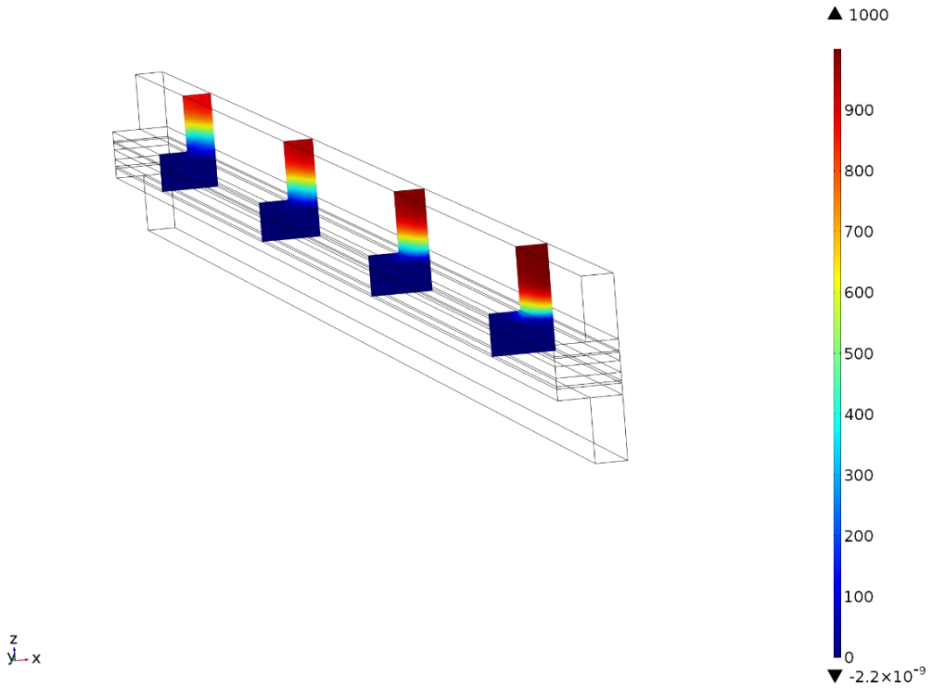

Fig. 4. Methanol concentration distribution.

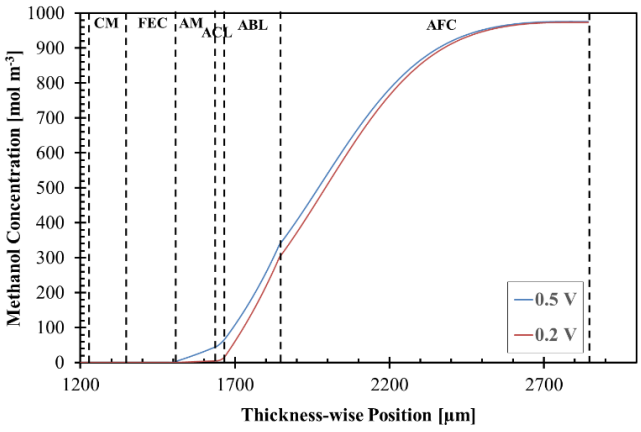

Fig. 5. Concentration of methanol at the mid of the symmetry axis along the thickness wise position (z direction) with different cell voltages.

In Fig. 6, the saturation distribution at a cell voltage of 0.2 V is shown. The saturation distribution at the mid of the symmetry axis along the thickness wise position (z direction) with different cell voltages (0.5 and 0.2 V) is shown in Fig. 7. The liquid saturation within the anode and FEC is very high, ~0.9, and constant for both cell voltages as shown in these figures. As the cell voltage descreases, the liquid saturation within the ACL decreases due to the consumption of methanol and water solution, and the production of carbon dioxide. At the lower cell voltage, 0.2 V, the liquid saturation decreases to a value of 0.894. The cathode also showed the same type of trend. However, in this case, the liquid saturation increases from a value of 0.11 to 0.127 at a cell voltage of 0.2 V. This increase in liquid saturation is owing to the combination of water crossover from the FEC to the cathode and due to the generation of water from the ORR and MOR from any crossed over methanol. In the FEC, saturation negligibly changes because of the lack of chemical reactions.

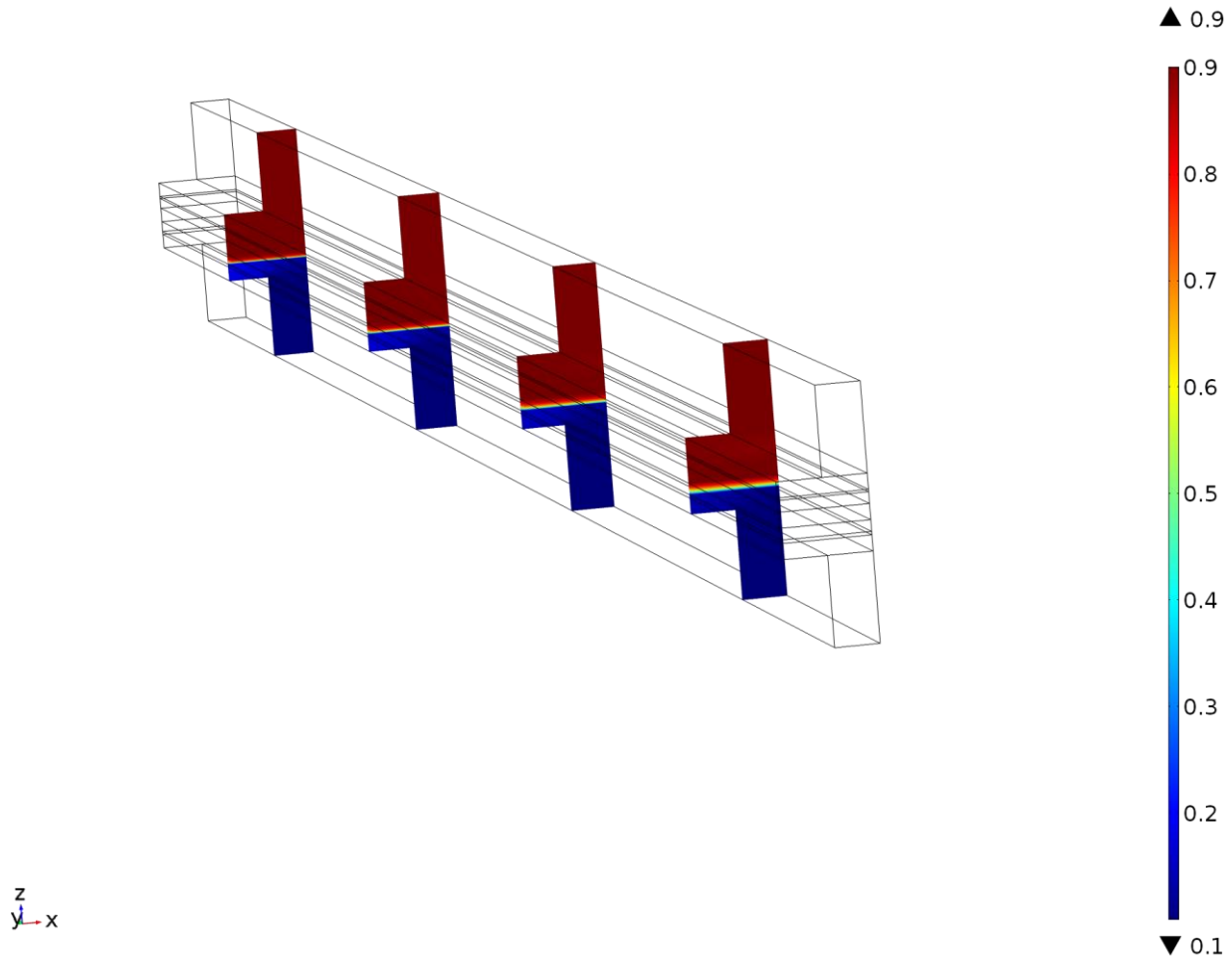

Fig. 6. Saturation distribution.

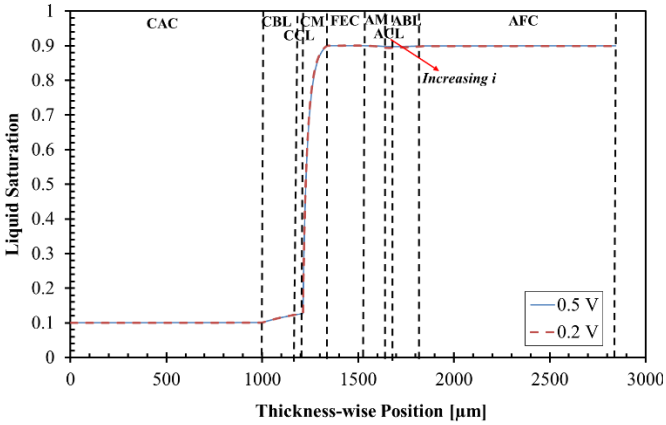

Fig. 7. Saturation distribution at the mid of the symmetry axis along the thickness wise position (z-direction) with different cell voltages.

III. II. Effect of FEC thickness on fuel cell power density

FEC thickness is one of the important parameters affecting the FE-DMFC performance. Therefore, the effect of four different thicknesses (0.175, 0.4, 0.6 and 0.8 mm) on the fuel cell power density is compared at 0.5 V as shown in Fig.8. it can be seen that the highest power density is obtained with 0.4 mm FEC thickness (533.3 W m^{-2}). When the FEC thickness is varied from 0.175 mm to 0.8 mm, ohmic losses go up, however, methanol crossover, which is the methanol transition from anode to the cathode, decreases. Therefore, the optimization of the FEC thickness needs to be done. It is also found that the increase in the power density is %13.2 (from 0.175 mm to 0.4 mm FEC thickness).

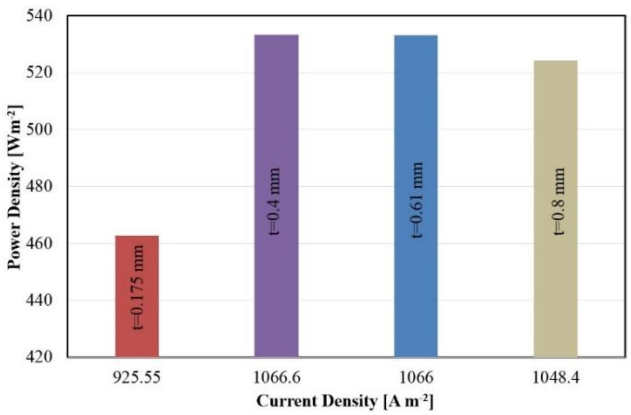

Fig. 8. Effect of FEC thickness on fuel cell power density.

IV. Conclusions

A three dimensional and two-phase FE-DMFC model has been developed to find its performance under given operating conditions. In order to develop this model, the commercial software, Comsol Multiphysics 5.0, has been used to solve the governing conservation equations of momentum, mass, species and charge numerically. Then, concentration of the methanol and liquid saturation distribution have been examined at the baseline condition. As a parametric study, the effect of FEC thickness has been investigated. Conducting this parametric study, power densities have been found for four FEC thicknesses. The results show that FEC thickness should be 0.4 mm for the given set of data. At this thickness, the negative effects of methanol crossover are minimized and the power density is maximized.

Acknowledgements

The funding for this project was received from the European Union's Horizon 2020 research and innovation programme under the Marie Sklodowska-Curie grant agreement No. 661579.

Nomenclature

Abbreviations

ABL	Anode backing layer
ACL	Anode catalyst layer
AFC	Anode fuel channel
AM	Anode membrane
CAC	Cathode air channel
CBL	Cathode backing layer
CCL	Cathode catalyst layer
CM	Cathode membrane
DMFC	Direct methanol fuel cell
FEC	Flowing electrolyte channel
FE-DMFC	Flowing electrolyte-direct methanol fuel cell
MFM	Multi fluid model
MMM	Multiphase mixture model

Greeks Letters

$\boldsymbol{\nu}$	Kinematic viscosity, $m^2\ s^{-1}$
σ	Surface tension, $N\ m^{-2}$
μ	Dynamic viscosity of fluid, $kg\ m^{-1}\ s^{-1}$
α	Transfer coefficient, unitless
ε	Porosity, unitless
η	Overpotential, V
κ	Permeability, m^2
ρ	Density, $kg\ m^{-3}$
σ	Conductivity, $S\ m^{-1}$
ϕ	Potential, V
γ	Advection correction factor, unitless
θ_c	Contact Angle, °
κ	Electrical conductance, $S\ m^{-1}$

Variables

a	Activity, unitless
ai_o	Reference exchange current density, $A\ m^{-3}$
C	Heat capacitance, $J\ kg^{-1}\ K^{-1}$
C_p	Heat capacitance, $J\ kg^{-1}\ K^{-1}$
D	Diffusion coefficient, $m^2\ s^{-1}$
$\boldsymbol{f}$	Body force, $N\ m^{-3}$
F	Faraday constant, $C\ mol^{-1}$
h	Enthalpy, $kJ\ mol^{-1}$
$\boldsymbol{I}$	Identity matrix
$\boldsymbol{i}$	Current density, $A\ m^{-2}$
j	Volumetric current density, $A\ m^{-3}$
J	Leverett J-Function, unitless
j_l	Capillary diffusion flux of liquid state, $kg\ m^{-2}\ s^{-1}$
j_{xover}	Crossover current density, $A\ m^{-3}$
k	Thermal conductivity, $W\ m^{-1}\ K^{-1}$
K_c	Reaction constant for methanol oxidation, $mol\ m^{-3}$
k_H	Henry's constant, unitless
M	Molecular weight, $kg\ mol^{-1}$
n_d	Coefficient of electro-osmotic drag, unitless
P	Pressure, Pa
R	Universal gas constant, $J\ mol^{-1}\ K^{-1}$
s	Liquid saturation, unitless
S_{gen}^k	Molar consumption/generation flux of species k, $mol\ m^{-3}\ s^{-1}$
S_{trans}	Transport source term, $kg\ m^{-3}\ s^{-1}$
T	Temperature, K
$\boldsymbol{u}$	Velocity, $m\ s^{-1}$
V	Cell voltage, V

Subscript/Superscript

a	Anode
c	Cathode
channel	Channel
e	Electrolyte phase
eff	Effective value
fg	Phase change
g	Gaseous/vapour state
H_2O	Water
in	Inlet
k	Species
l	Liquid phase
lg	Two-phase condition
mem	Membrane
MeOH	Methanol
O_2	Oxygen
out	Outlet
ref	Reference value
Ref	Reference
s	Solid phase
xover	Crossover

References

Atacan, O. F., Ouellette, D., & Colpan, C. O. Two dimensional multiphase non-isothermal modeling of a flowing electrolyte–direct methanol fuel cell. *International Journal of Hydrogen Energy*, *42*(4), 2669-2679, (2017).

Kakaç, S., Pramuanjaroenkij, A., & Vasiliev, L. (Eds.). *Mini-micro fuel cells: Fundamentals and applications*. Springer Science & Business Media, (2008).

Colpan, C. O., Cruickshank, C. A., Matida, E., & Hamdullahpur, F. 1D modeling of a flowing electrolyte-direct methanol fuel cell. *Journal of Power Sources*, *196*(7), 3572-3582, (2011).

Colpan, C. O., Cruickshank, C. A., Matida, E., & Hamdullahpur, F., 1D modeling of a flowing electrolyte-direct methanol fuel cell. *Journal of Power Sources*, *196*(7), 3572-3582, (2011).

Colpan, C. O., Ouellette, D., Glüsen, A., Müller, M., & Stolten, D. Reduction of methanol crossover in a flowing electrolyte-direct methanol fuel cell. *International Journal of Hydrogen Energy*, (2017).

Duivesteyn, E., Cruickshank, C. A., & Matida, E. Modelling of a porous flowing electrolyte layer in a flowing electrolyte direct-methanol fuel cell. *International Journal of Hydrogen Energy*, *38*(30), 13434-13442, (2013).

Duivesteyn, E., Cruickshank, C. A., & Matida, E. Nonisothermal Hydrodynamic Modeling of the Flowing Electrolyte Channel in a Flowing Electrolyte–Direct Methanol Fuel Cell. *Journal of Fuel Cell Science and Technology*, *11*(2), 021011, (2014).

Jung, S. Non-isothermal multi-dimensional direct methanol fuel cell model with micro-porous layers mitigating water/methanol crossover. *Journal of Power Sources*, *231*, 60-81, (2013).

Kablou, Y., Cruickshank, C. A., & Matida, E. Experimental analysis of a small-scale flowing electrolyte–direct methanol fuel cell stack. *Journal of Fuel Cell Science and Technology*, *12*(4), 041007, (2015).

Kjeang, E., Goldak, J., Golriz, M. R., Gu, J., James, D., & Kordesch, K. Modeling Methanol Crossover by Diffusion and Electro - Osmosis in a Flowing Electrolyte Direct Methanol Fuel Cell. *Fuel Cells*, *5*(4), 486-498, (2005).

Kjeang, E., Goldak, J., Golriz, M. R., Gu, J., James, D., & Kordesch, K. (2006). A parametric study of methanol crossover in a flowing electrolyte-direct methanol fuel cell. *Journal of Power Sources*, *153*(1), 89–99. https://doi.org/10.1016/j.jpowsour.2005.03.181

Kordesch, K., Hacker, V., & Bachhiesl, U. Direct methanol–air fuel cells with membranes plus circulating electrolyte. *Journal of Power Sources*, *96*(1), 200–203, (2001).

Kjeang, E., Goldak, J., Golriz, M. R., Gu, J., James, D., & Kordesch, K. Modeling Methanol Crossover by Diffusion and Electro - Osmosis in a Flowing Electrolyte Direct Methanol Fuel Cell. *Fuel Cells*, *5*(4), 486-498, (2005).

O Ouellette, D., Colpan, C. O., Cruickshank, C. A., & Matida, E. Parametric studies on the membrane arrangement and porous properties of the flowing electrolyte channel in a flowing electrolyte–direct methanol fuel cell. *International Journal of Hydrogen Energy*, *40*(24), 7732-7742, (2015).

Ouellette, D., Colpan, C. O., Matida, E., & Cruickshank, C. A. A single domain approach to modeling the multiphase flow within a flowing electrolyte–direct methanol fuel cell. *International Journal of Hydrogen Energy*, *40*(24), 7817-7828, (2015).

Ouellette, D., Colpan, C. O., Matida, E., Cruickshank, C. A., & Hamdullahpur, F. A comprehensive 1D model of a flowing electrolyte - direct methanol fuel cell with experimental validation. *International Journal of Energy Research*, *39*(1), 33-45, (2015).

Sabet-Sharghi, N., Cruickshank, C. A., Matida, E., & Hamdullahpur, F. Performance measurements of a single cell flowing electrolyte-direct methanol fuel cell (FE-DMFC). *Journal of Power Sources*, *230*, 194-200, (2013).

Wang, Z. H., & Wang, C. Y. (2003). Mathematical modeling of liquid-feed direct methanol fuel cells. *Journal of The Electrochemical Society*, *150*(4), A508-A519.